Article

Not peer-reviewed version

# Enhancement of Low-Density Coal Recovery Through Controlled Comminution Strategies

Quentin Peter Campbell , Marco Le Roux , Fardis Nakhaei *

Posted Date: 13 May 2025

doi: 10.20944/preprints202505.0954.v1

Keywords: coal yield; compressive breakage; impact breakage; attrition; liberation

 doi:10.20944/preprints202505.0954.v1



*Article*

# Enhancement of Low-Density Coal Recovery Through Controlled Comminution Strategies

**Quentin Peter Campbell, Marco Le Roux and Fardis Nakhaei ***

School of Chemical and Minerals Engineering, North-West University, Potchefstroom 2531, South Africa

* Correspondence: fardis.nakhaei@mst.edu

**Abstract:** Coal resources, such as those from the South African Waterberg coal field and the Mozambique coalfields, often contain highly interlayered structures of coal macerals and mineral matter. The mineral matter, which is incombustible, reduces the coal's calorific value and poses challenges during coal processing due to its adverse impact on plant yields. Effective liberation of coal from mineral matter is crucial to maximize economic recovery and reduce undesirable ash content. This study investigates the effect of various breakage modes on the liberation of coal to attain a high yield of low-ash coal. Coal samples from the Moatize Coalfield in Mozambique were subjected to impact breakage, compressive breakage, and attrition breakage in different combinations to determine the optimal conditions for maximizing coal yield while minimizing fines formation. The results showed that impact breakage to a top size of 6.7 mm followed by attrition breakage significantly enhanced the coal yield, particularly for material with relative density (RD) <1.4. The study also identified an optimal particle size of 4.75 mm, where the cumulative yield of liberated coal with RD <1.4 was maximized. The most effective combination for improving coal yield was impact breakage to 6.7 mm, followed by a short attritioning time of 1 minute. This combination achieved a yield of 61%, a significant increase compared to the raw coal yield of 26%. The findings highlight the importance of breakage mode selection and particle size for optimizing coal liberation and yield in processing plants.

**Keywords:** coal yield; compressive breakage; impact breakage; attrition; liberation

## 1. Introduction

Comminution is a fundamental step in coal processing, responsible for reducing particle size and liberating coal macerals from mineral matter to enhance beneficiation efficiency. This process typically involves a sequence of mechanical operations, including crushing and fine grinding with equipment such as ball mills, stirred media mills, or IsaMills. As one of the most energy-intensive stages, comminution can contribute up to 70% of the total energy consumption in a mineral processing plant [1,2]. More specifically, fine grinding and ultra-fine processing account for approximately 80%–90% of this energy usage, whereas the crushing stage generally consumes only 5% to 7% of the total comminution energy [3,4]. Therefore, improving comminution efficiency is vital to minimizing operational costs and enhancing overall plant performance.

Despite the declining global dependence on coal as a fuel, its role remains significant in specific regions for power generation and in industrial applications such as the production of metallurgical coke and anode-grade carbon materials. Additionally, the potential recovery of critical elements from coal and its byproducts has renewed interest in coal utilization beyond combustion [5,6]. These developments emphasize the need to revisit and refine coal processing strategies to adapt to both emerging economic opportunities and sustainability goals.

Although interest in alternative energy sources continues to rise, fossil fuels remain the dominant contributors to global electricity generation. As of 2023, oil accounted for about 32.0% of worldwide energy use, followed by coal at 27.0% and natural gas at 24.0%, together making up approximately 83.0% of the global energy portfolio [7]. Coal is South Africa's primary energy source,

 doi:10.20944/preprints202505.0954.v1



accounting for more than 85% of the country's electricity generation through coal-fired thermal power plants [8]. The thermal efficiency of combustion-based systems is closely tied to the quality of coal feedstock [9,10]. Increasing heterogeneity and reduced quality of accessible coal resources—characterized by complex intergrowths of macerals and mineral matter—have increased the energy requirements for effective liberation [11,12].

In coal cleaning, the primary objective of separation is to increase the concentration of combustible organic material while reducing inorganic gangue minerals. This improves the calorific value of coal and reduces harmful emissions during combustion [13]. The process begins with controlled comminution to avoid excessive fines, followed by size classification using screens or hydrocyclones. Gravity-based methods such as jigs, dense medium separators, and spirals are widely applied due to their simplicity and cost-effectiveness. For finer particles, surface-based techniques like flotation are preferred, utilizing differences in surface wettability to separate hydrophobic coal from hydrophilic minerals [14,15]. Column flotation and oil agglomeration are further employed for ultra-fine coal, where conventional methods may be less effective [16].

A significant challenge in coal beneficiation is the control of fine particle generation during grinding. It is usually desirable to minimize the amount of fines (particles finer than ~0.5 mm) produced in size reduction due to their adverse impact on dewatering, handling, and separation performance [17]. Moreover, they tend to reduce flotation selectivity and recovery rates and are prone to entrainment losses. In this context, comminution must strike a balance between achieving sufficient liberation for separation and minimizing excessive fines production [18,19]. This calls for coal to be processed at the coarsest feasible particle size that still permits effective liberation [20].

Coal's breakage behavior is influenced by its mineralogical composition, microstructural complexity, and the mechanical properties of both the coal matrix and the embedded mineral matter. For example, coals with large, discrete mineral inclusions can be selectively liberated with limited size reduction. In contrast, finely disseminated mineral matter requires extensive grinding to expose and separate the mineral phases [21,22]. This microstructural variability underscores the importance of tailoring breakage strategies to deposit-specific coal characteristics. Effective liberation of coal from mineral matter is essential for improving product quality and ensuring high recovery rates in physical separation processes such as density-based separation and flotation.

Understanding the breakage characteristics of coal is essential for optimizing liberation while minimizing the production of coal fines. Different breakage mechanisms—impact, compression, and attrition—induce distinct stress regimes that influence how particles fracture [23,24]. Impact breakage often causes tensile failure, promoting shattering and rapid size reduction. Compression results in bulk fracture under applied pressure, while attrition generates wear and surface abrasion through particle-particle or particle-wall interactions. Each mechanism can lead to different degrees and patterns of mineral liberation, depending on coal texture and composition [25].

Despite the significance of comminution in mineral and coal processing, current literature tends to focus more on equipment performance modeling and simulation than on the fundamental fracture behavior of granular coal systems under various stress modes [26–29]. The mechanical response of composite particles to different types of forces remains insufficiently explored. Recent advances in digital particle tracking, micro-CT imaging, and discrete element modeling (DEM) offer promising avenues for better understanding fracture propagation, but their application to coal remains limited. In addition to mechanical methods, several alternative approaches have been investigated to improve mineral liberation, particularly in low-grade ores where grinding energy demands are high. These include thermal pretreatment, chemical additives, microwave irradiation, and electro-pulse disintegration [30–35]. Although these techniques have shown potential in laboratory studies, their scalability and economic viability remain significant barriers to industrial adoption. There is therefore a continuing need to explore innovative breakage strategies within conventional mechanical systems to enhance liberation while maintaining energy efficiency.

This study evaluates the effectiveness of various breakage mechanisms in achieving optimal coal liberation while minimizing the generation of fine particles. Coal samples sourced from the Moatize

 doi:10.20944/preprints202505.0954.v1



Coalfield in Mozambique were subjected to a sequential application of impact, compressive, and attrition breakage to determine the most effective combination for maximizing yield at coarse particle sizes. By establishing the relationship between breakage mechanism and liberation behavior, the findings offer valuable insights for the design of more efficient and sustainable coal beneficiation circuits.

## 2. Experimental Procedures

*2.1. Materials*

The coal samples used in this study were sourced from the Chipanga Seam of the Moatize Coalfield in Mozambique, a region well-documented for its complex and highly stratified morphology. This coal seam is characterized by extensive interlayering of organic macerals with a diverse suite of mineral matter, including quartz, kaolinite, and carbonates, which presents significant challenges in terms of liberation and beneficiation. The parallel laminar structure of the coal particles, indicative of sedimentary depositional layering and post-depositional compaction, is visually evident in the photomicrograph provided in Figure 1. Such textural complexity necessitates a carefully designed comminution strategy to effectively liberate coal from its associated mineral matrix.

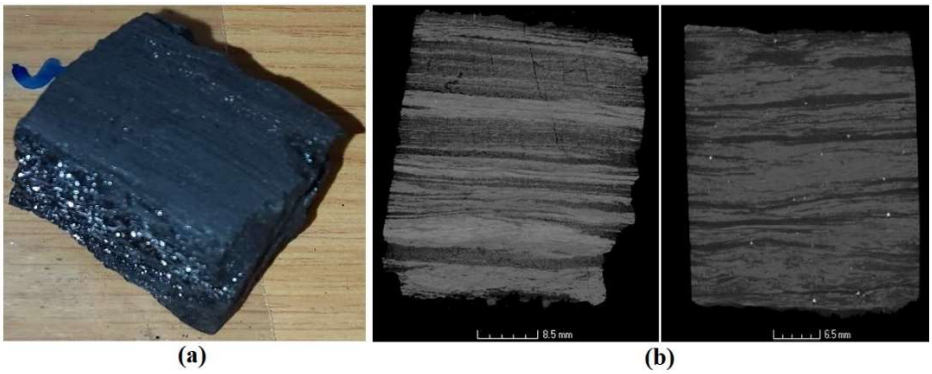


**Figure 1.** Micro-focus X-ray computed tomography image of a coal sample from the Chipanga Seam, Moatize Coalfield, Mozambique.

The particle size distribution of the raw coal sample was first established through a staged screening process, with the top size set at 75 mm (Figure 2). Washability analysis was subsequently conducted on each size fraction to assess the distribution of material across varying relative density classes (Table 1). The sample exhibited a mass-based median particle size ($D_{50}$) of approximately 16 mm, with only a small fraction (4.3%) of the total mass falling below 0.5 mm.

Notably, the coarsest size fraction (53–75 mm) contained no material within the low-density intervals (<1.6), indicating a lack of liberated coal in this fraction. Instead, 3.7% and 4.5% of the total sample mass in this size class were distributed in the 1.6–1.7 and 1.7–1.8 relative density ranges, respectively. This trend implies that the coarse particles are primarily associated with higher mineral matter content, as higher relative densities are typically indicative of denser, inorganic constituents.

Coal particles with relative densities below 1.4 are typically classified as clean coal, whereas those with densities exceeding 1.8 are generally associated with mineral-rich material. In the present study, material within the ≥1.8 relative density class constitutes approximately 22.8% of the total sample mass, with a substantial portion located in the 9.5–75.0 mm size range. This trend suggests that the coarser size fractions are notably enriched in mineral matter, reinforcing the need for additional comminution to promote sufficient liberation and facilitate more effective physical separation. Material falling within the intermediate relative density range of 1.4–1.8, which includes both potential clean coal and middlings, is distributed across all size fractions but is especially concentrated in the 6.7–75.0 mm range. This distribution highlights the compositional heterogeneity and textural complexity of the raw coal, where organic macerals are intricately intergrown with

 doi:10.20944/preprints202505.0954.v1



inorganic mineral matter. Efficient separation of this material is inherently challenging and necessitates strategically applied breakage mechanisms to enhance liberation while minimizing the loss of valuable coal to high-density fractions.

In contrast, finer size fractions (particularly <4.75 mm) exhibit a greater proportion of low-density material, especially within the 1.3 and 1.3–1.4 density ranges. These fractions are enriched in liberated coal and collectively account for approximately 21.8% of the total sample mass. Given their higher degree of inherent liberation—resulting from mining-induced breakage and degradation during transport—these fine particles generally require minimal additional comminution. Their favorable washability characteristics make them highly amenable to separation processes, which is advantageous for improving overall plant yield and product quality.

The overall washability distribution reveals that 22.8% of the total sample is associated with the >1.8 relative density class, indicating a considerable presence of high-density, mineral-rich material. Additionally, a combined 54.8% of the sample falls within the 1.4–1.8 relative density range, representing a substantial portion of middling or composite particles containing variable proportions of coal macerals and mineral matter. In contrast, only 5.82% and 16.0% of the material fall within the <1.3 and 1.3–1.4 density intervals, respectively—ranges typically indicative of clean coal with low ash content.

These findings highlight the predominance of higher-density and composite materials in the raw feed, underscoring the need for a carefully optimized comminution and density-based separation strategy to enhance liberation and maximize the recovery of clean coal, while minimizing ash content in the final product.

**Table 1.** The washability of the raw coal sample across different size fractions.

| Size (mm) | Relative density | | | | | | | Total |
|---|---|---|---|---|---|---|---|---|
| | 1.3 | 1.3-1.4 | 1.4-1.5 | 1.5-1.6 | 1.6-1.7 | 1.7-1.8 | >1.8 | |
| 53-75 | 0.00 | 0.00 | 0.00 | 0.00 | 3.66 | 4.53 | 0.00 | 8.19 |
| 37.5 -53 | 0.00 | 3.33 | 3.80 | 2.01 | 0.00 | 0.00 | 3.89 | 13.03 |
| 26.5-37.5 | 0.00 | 0.00 | 0.93 | 2.11 | 2.70 | 0.97 | 2.87 | 9.58 |
| 19-26.5 | 0.00 | 1.01 | 2.22 | 2.40 | 0.92 | 1.84 | 3.23 | 11.62 |
| 13.2-19 | 0.00 | 1.28 | 3.26 | 1.65 | 0.90 | 1.04 | 4.08 | 12.21 |
| 9.5-13.2 | 0.09 | 0.76 | 1.71 | 0.89 | 0.96 | 0.34 | 2.16 | 6.91 |
| 6.7-9.5 | 0.19 | 1.10 | 2.00 | 1.12 | 0.61 | 0.49 | 1.66 | 7.07 |
| 4.75-6.7 | 1.02 | 0.92 | 1.46 | 0.91 | 0.58 | 0.47 | 1.42 | 6.58 |
| 2-4.75 | 2.10 | 2.05 | 1.96 | 1.03 | 0.60 | 0.44 | 1.75 | 10.43 |
| 1-2 | 2.42 | 1.88 | 0.72 | 0.53 | 0.42 | 0.15 | 0.88 | 7.00 |
| 0.5-1 | 0.00 | 1.71 | 0.17 | 0.44 | 0.05 | 0.08 | 0.26 | 2.71 |
| 0-0.5 | 0.00 | 1.99 | 0.45 | 1.00 | 0.12 | 0.12 | 0.59 | 4.27 |
| Total | 5.82 | 16.03 | 18.68 | 14.09 | 11.52 | 10.47 | 22.79 | 100 |

 doi:10.20944/preprints202505.0954.v1



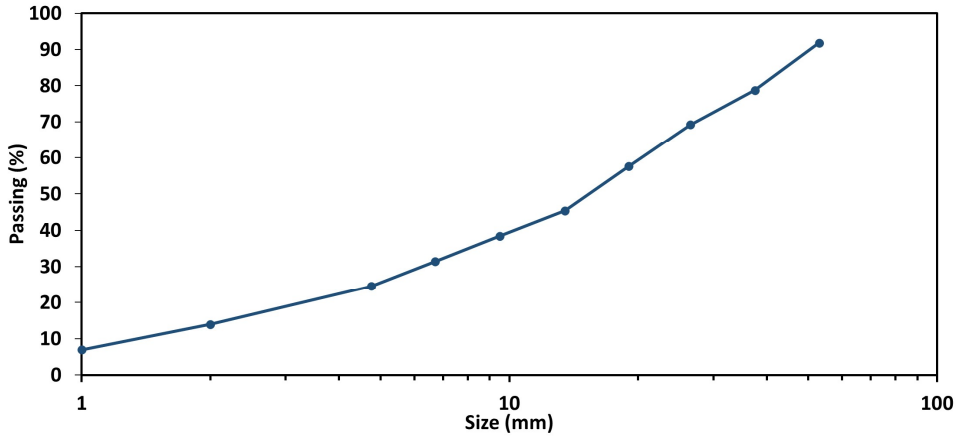


**Figure 2.** Particle size distribution of the coal sample from the Moatize Coalfield.

Table 2 presents the results of proximate analysis, calorific value, and free swelling index (FSI) for the bulk coal sample, categorized by relative density intervals. The data reveal a clear and consistent deterioration in coal quality with increasing density. The low-density fractions (<1.3 and 1.3–1.4) exhibit the most desirable properties, including low ash content (4.5% and 12.8%, respectively), high fixed carbon content (76.4% and 69.7%), and elevated calorific values of 34.2 and 30.7 MJ/kg. These fractions also show the highest FSI values (7.5 and 4), indicating good coking potential.

In contrast, the high-density fractions (>1.6) are associated with significantly reduced coal quality. The ash content progressively increases from 35.5% (1.6–1.7) to 59.2% (>1.8), while fixed carbon content declines from 50.2% to 24.8%, and calorific value drops sharply from 21.9 MJ/kg to 10.6 MJ/kg. The total sulfur content also peaks at 1.7% in the >1.8 fraction, further confirming the enrichment of mineral matter in higher-density components.

These findings emphasize the importance of effective liberation and particle characterization in improving the performance of density-based separation processes. The sharp contrast in compositional attributes between low- and high-density fractions supports the selective rejection of mineral-rich material and highlights the potential for optimizing clean coal recovery through targeted comminution and precise classification.

**Table 2.** Proximate, calorific value and free swelling index analysis results.

| Density | Ash (%) | Volatile Matter (%) | Fixed Carbon (%) | Calorific Value (MJ/kg) | Total Sulphur (%) | Free Swelling Index |
|---|---|---|---|---|---|---|
| <1.3 | 4.47 | 19.19 | 76.35 | 34.18 | 0.98 | 7.5 |
| 1.3-1.4 | 12.8 | 17.48 | 69.72 | 30.67 | 0.9 | 4 |
| 1.4-1.5 | 19.72 | 16.46 | 63.82 | 28.14 | 0.9 | 2.5 |
| 1.5-1.6 | 27.05 | 15.5 | 57.45 | 25.05 | 0.82 | 1 |
| 1.6-1.7 | 35.47 | 14.33 | 50.2 | 21.94 | 0.8 | 0 |
| 1.7-1.8 | 44.26 | 13.1 | 42.64 | 18.38 | 0.86 | 0 |
| >1.8 | 59.22 | 12.93 | 24.85 | 10.64 | 1.7 | 0 |

 doi:10.20944/preprints202505.0954.v1



*2.2. Experimental Design and Breakage Strategy*

The bulk coal sample was thoroughly homogenized and subsequently divided into a series of representative sub-samples, each weighing approximately 6 kg, using the cone and quartering method—a widely accepted technique for preserving sample integrity and minimizing selection bias in particulate materials. To minimize particle degradation and the artificial generation of fines, manual screening was applied wherever possible in lieu of mechanical methods.

Following particle size classification, a series of controlled breakage experiments were conducted to evaluate the effects of distinct breakage mechanisms on coal yield, liberation characteristics, and particle size distribution. These experiments were designed to simulate operational conditions and assess the efficiency of breakage modes under varying energy inputs.

Figure 3 summarizes the experimental framework, detailing the specific breakage modes, selected top particle sizes, and the extent of attrition-induced breakage over different residence times following the primary size reduction step. The selection of top particle sizes was informed by industrial best practices and aimed to balance the need for sufficient liberation with the necessity to limit excessive fines generation, which can compromise product quality and complicate downstream processing operations.

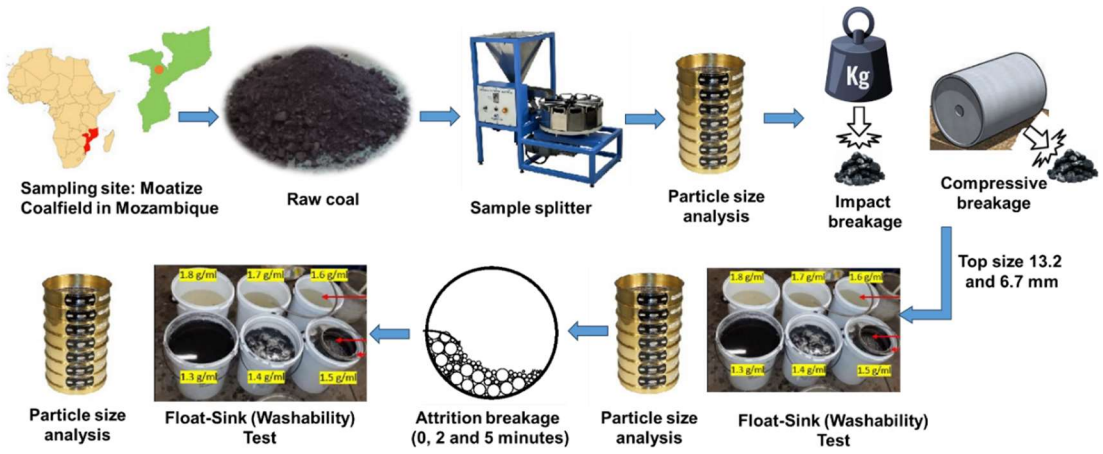


**Figure 3.** Fellow diagram of steps performed during impact breakage.

The coal samples were individually subjected to breakage testing in accordance with SANS 401:2010, the Standard Test Method for Drop Shatter Test for Coal, using a custom-designed drop-weight impact rig (Figure 4a). Each sub-sample was randomly arranged in a single-layer configuration at the base of the rig to ensure consistent exposure to impact. A 14.65 kg steel plate, secured in position by a safety pin, was released from a fixed height of 1.8 m, imparting a standardized impact force to facilitate particle breakage. A centrally aligned steel guide pipe ensured the vertical descent of the plate, providing uniform and reproducible impact conditions across all tests.

For the compressive breakage experiments, a distinct setup was employed involving a manually operated 80 kg lawn roller in combination with a steel-framed platform (Figure 4b). Coal particles were again arranged randomly in a single layer over a surface area of 2.0 m × 0.5 m. The lawn roller was manually traversed across the platform to apply compressive force, simulating the breakage mechanism typically encountered in low-energy compaction or handling scenarios. This approach allowed for the comparative evaluation of impact versus compressive stress regimes on particle size reduction and liberation behavior.

 doi:10.20944/preprints202505.0954.v1



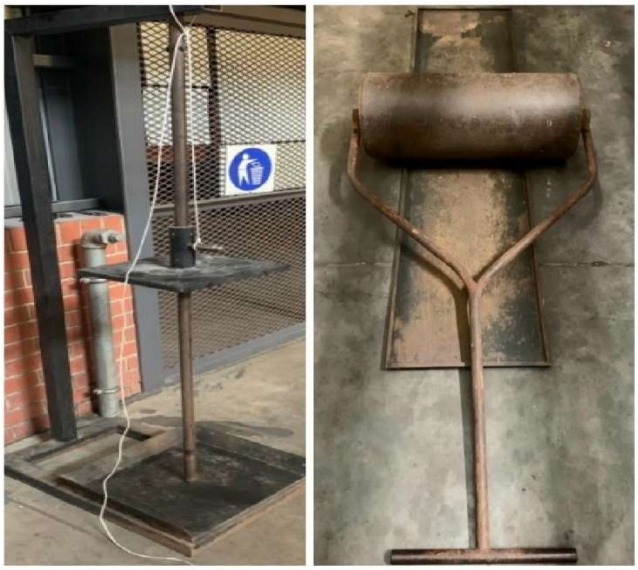

(a) (b)

**Figure 4.** (a) Drop-weight impact rig used for conducting the drop shatter test. (b) Lawn roller and steel frame setup employed for compressive breakage experiments.

Following breakage, the fragmented coal samples were screened using sieves with aperture sizes corresponding to the designated top sizes of 6.7 mm or 13.2 mm. Oversized particles that did not pass through the respective sieves were returned to their original setup for additional impact or compressive breakage until the target size reduction was fully achieved. The resulting data will be used to assess the influence of top particle size on the degree of liberation from mineral matter, as well as its effect on enhancing overall coal yield.

The breakage experiments were conducted under two conditions: without attrition and with additional attrition stages of 2 and 5 minutes. The attrition breakage was performed using a tumbling mill with an internal diameter of 38.5 cm and a length of 50 cm, operated without any grinding media. The mill was rotated at 20 rpm, equivalent to 30% of the calculated critical speed, to promote a cascading motion and minimize excessive breakage from impact forces. This setup was designed to simulate low-energy attrition conditions, allowing for a controlled evaluation of the effect of secondary breakage on particle size distribution and coal liberation.

Particle size distribution and washability analyses were performed on each sample both prior to and following each breakage experiment. Among the available techniques to assess coal liberation and separation performance, the float-sink test remains a robust and widely adopted method. This technique evaluates the density distribution of size fractions following comminution and offers insights into the degree of liberation and potential yield. Densiometric analysis was conducted using zinc chloride ($ZnCl_2$) solutions, with a relative density (RD) of 2.91. A series of $ZnCl_2$ solutions with RDs ranging from 1.3 to 1.8, in increments of 0.1, were prepared to facilitate the separation of particles based on their density. The coal sample was initially introduced into the lowest-density solution (RD 1.30), allowing sufficient time for particle separation into float and sink fractions. The floating particles were collected using a hand sieve and thoroughly rinsed with water to remove residual $ZnCl_2$. The remaining sunk fraction was then transferred to the next higher-density solution (RD 1.40), and the process was repeated sequentially for each density increment until the final solution (RD 1.8) was reached. This stepwise separation approach enabled the generation of detailed density-based fractionation data for washability assessment.

The relative densities of the coal particles were subsequently correlated with their corresponding ash yields, as determined by proximate analysis. By quantifying ash content across the various relative density intervals, it is possible to infer the distribution of mineral matter throughout the sample. This correlation enables a more comprehensive understanding of the relationship between

 doi:10.20944/preprints202505.0954.v1



coal quality and density, thereby supporting the evaluation of liberation efficiency and the optimization of density-based separation strategies.

## 3. Results

This study investigates the effects of impact and compressive breakage in achieving target top particle sizes of 13.2 mm and 6.7 mm, followed by controlled attrition stages, on representative coal samples. Particular emphasis is placed on evaluating the resulting size-by-washability distribution and the extent of coal liberation as a function of attrition duration. The analysis primarily targets material with a relative density (RD) of ≤1.4, which is indicative of relatively clean coal composed predominantly of liberated macerals with minimal mineral matter inclusion. This fraction serves as a key indicator of separation efficiency and clean coal recovery potential under varying breakage conditions.

### *3.1. Effect of Impact and Attrition Breakage on Size-by-Washability Distribution*

#### 3.1.1. Top Particle Size of 13.2 mm

Figure 5 presents the size-by-washability distribution of coal subjected to impact breakage alone, targeting a top particle size of 13.2 mm, prior to any secondary attrition. The results indicate that impact breakage alone yields limited liberation of coal macerals from associated mineral matter. Specifically, the proportion of particles with a relative density (RD) ≤ 1.3, typically representative of clean coal, was only 6.30% of the total sample. However, the application of 2 and 5 minutes of attrition resulted in a marked improvement, increasing the RD ≤ 1.3 fraction to 8.60% and 8.85%, respectively (Figures 6 and 7). Similarly, the 1.3–1.4 RD fraction increased from 18.87% (no attrition) to 24.2% (2 minutes), followed by a slight decrease to 23.1% after 5 minutes. These findings suggest that attrition promotes effective coal liberation, primarily through selective abrasion and surface wear, rather than indiscriminate size reduction. This is further supported by the observation that most low-density material was concentrated in the 0.5–4.75 mm size range.

The generation of ultra-fines (<0.5 mm) remained modest across all test conditions, increasing only from 10.7% (no attrition) to 11.1% (2 minutes) and 11.7% (5 minutes). These small increments suggest that attrition promotes selective breakage, primarily through surface abrasion and natural fracture planes, rather than causing extensive size reduction. This controlled fragmentation enhances coal–mineral liberation while minimizing overgrinding and maintaining process efficiency by limiting fine particle generation.

Under the no-attrition condition, the high-density fraction (RD ≥ 1.8) accounted for 33.3% of the sample mass, with a substantial 17.9% concentrated in the coarsest size class (9.5–13.2 mm). This confirms that mineral-rich aggregates resist fragmentation during primary impact breakage and remain in the coarse fraction. After 2 minutes of attrition, this value dropped to 12.9%, indicating that attrition effectively disintegrated coarse, dense particles into smaller, more separable size classes. The total RD ≥ 1.8 fraction decreased to 30.6%, and further reduced to 29.7% after 5 minutes of attrition, confirming progressive disaggregation of mineral matter with extended attrition duration.

A notable shift in washability distribution was observed within the intermediate-density fractions. Specifically, the mass percentage in the 1.5–1.6 relative density interval increased substantially from 3.4% to 9.6% after 2 minutes of attrition, after which it remained relatively stable following 5 minutes of attrition. These shifts are accompanied by a significant reduction in the 1.4–1.5 RD fraction—from 27.1% (no attrition) to 14.8% (2 min) and 17.5% (5 min)—indicating that many particles in the middling zone transitioned toward either cleaner or more mineral-rich fractions, reflecting partial liberation and improved separability.

Overall, the cumulative yield of material with RD ≤ 1.4—a proxy for relatively clean coal—increased from 25.17% (no attrition) to 32.79% (2 min) and 31.93% (5 min). While this reflects enhanced liberation, the marginal gain between 2 and 5 minutes suggests diminishing returns with extended attrition.

 doi:10.20944/preprints202505.0954.v1



Concurrently, the coarsest size class (9.5–13.2 mm) reduced from 37.10% to 28.52% (2 min) and 24.07% (5 min), while the 1–4.75 mm range grew, confirming that coarse particles progressively fractured into mid-sized fragments during attrition. This redistribution is beneficial for density-based separation, where intermediate-size liberated particles are more readily processed without entrainment losses or misplacement.

In summary, 2 minutes of attrition appears to strike an optimal balance: it significantly enhances coal liberation, reduces coarse mineral aggregates, and maintains controlled fine generation. Extending attrition to 5 minutes yields only minor additional liberation while increasing energy input and the risk of overgrinding, which could compromise downstream beneficiation performance.

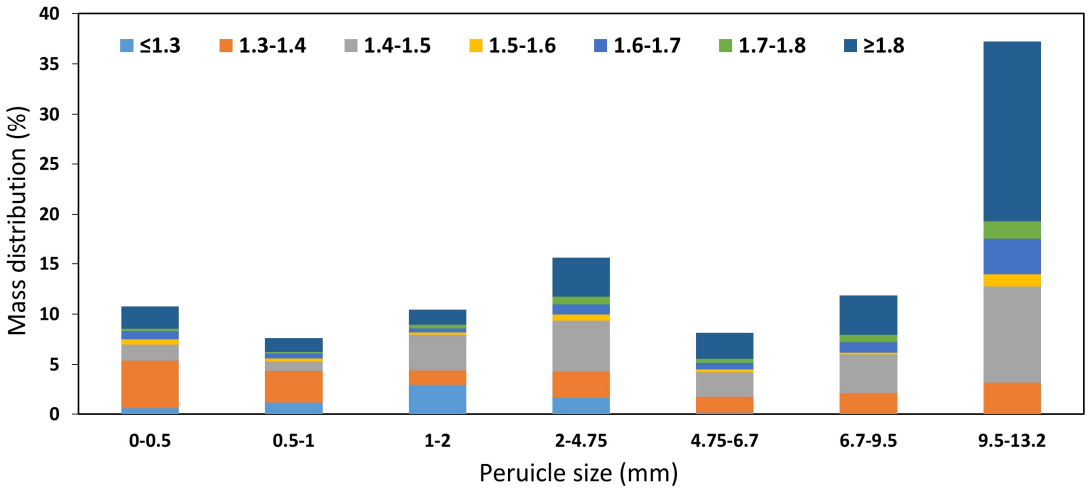


**Figure 5.** Size-by-washability distribution of coal subjected to impact breakage to a top particle size of 13.2 mm prior to any additional attrition treatment.

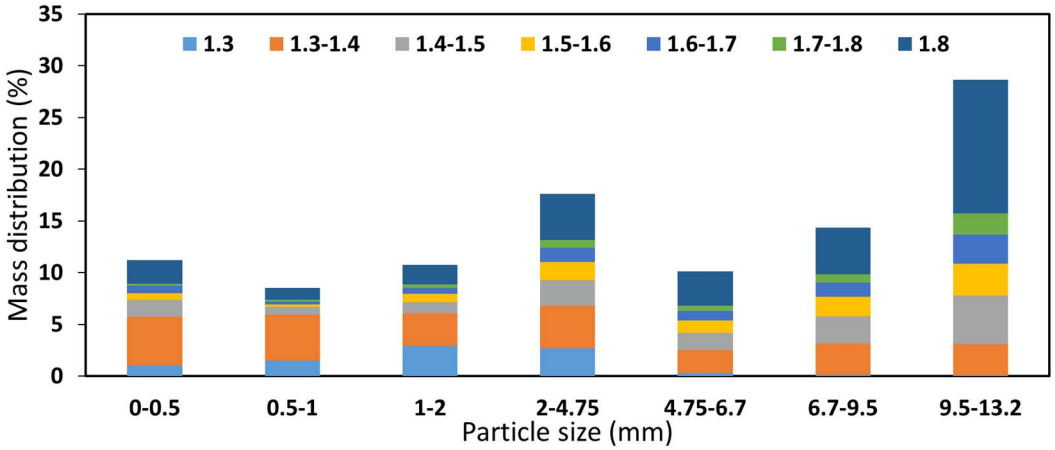


**Figure 6.** Size-by-washability distribution of coal subjected to impact breakage to a top particle size of 13.2 mm, followed by 2 minutes of attrition breakage.

 doi:10.20944/preprints202505.0954.v1



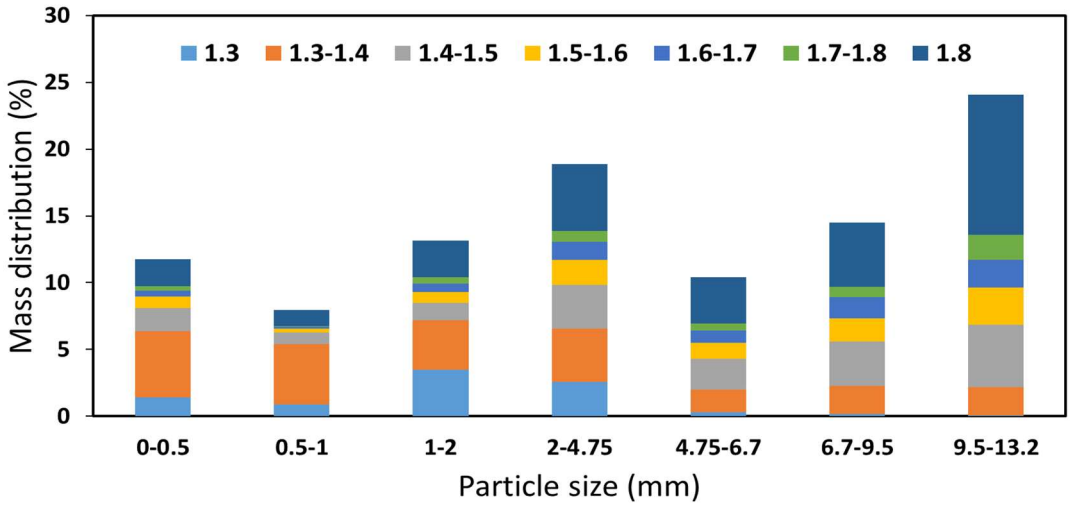


**Figure 7.** Size-by-washability distribution of coal subjected to impact breakage to a top particle size of 13.2 mm, followed by 5 minutes of attrition breakage.

### 3.1.2. Top Particle Size of 6.7 mm

Coal samples were subjected to controlled impact breakage to achieve a top particle size of 6.7 mm, followed by 0, 2, and 5 minutes of attrition (Figures 8–10). The results were benchmarked against those obtained at a coarser 13.2 mm top size to assess the role of particle size in coal liberation.

Following impact breakage to 6.7 mm, the mass fraction of coal particles with relative density (RD) ≤ 1.3 was 9.6%, an increase from 6.3% observed at the 13.2 mm top size. Similarly, the cumulative RD < 1.4 fraction rose from 25.2% to 34.5%, indicating substantially improved liberation of macerals at finer particle sizes. This enhancement is attributed to greater exposure of coal-mineral boundaries and increased internal stresses that promote fracture along mineral interfaces.

The 1.3–1.4 RD class also rose from 18.9% (13.2 mm) to 24.9% (6.7 mm), highlighting the increased generation of partially liberated particles. The <0.5 mm size fraction also increased from 10.7% (13.2 mm) to 17.2% (6.7 mm) after impact breakage, suggesting more extensive surface fragmentation. Within the <0.5 mm size fraction, the content of RD < 1.4 material increased from 7.47% (no attrition) to 10.37% after 2 minutes of attrition, and further to 11.20% after 5 minutes, reinforcing the conclusion that finer breakage followed by attrition enhances maceral liberation, particularly through detachment from dense mineral matrices.

Despite the improved liberation, a significant middling fraction (RD 1.4–1.8) persisted. At top size 6.7 mm, this group accounted for 36.7%, down from 42.8% at 13.2 mm. Moreover, the middlings in the coarsest fraction (4.75–6.7 mm for 6.7 mm top size, and 6.7–13.2 mm for 13.2 mm) dropped from ~21.9% to ~18.4%, implying that finer breakage exposes embedded macerals, making them more amenable to separation.

Two minutes of attrition significantly enhanced liberation. The RD ≤ 1.3 fraction rose from 9.6% to 13.8%, and RD < 1.4 reached 39.3%, compared to 25.1% under the same treatment at a 13.2 mm top size. This confirms that smaller initial particle sizes maximize attrition efficiency by presenting more exposed interfaces for abrasion and micro-fracturing. Concurrently, the ≥ 1.8 RD fraction declined from 29.3% to 23.6%, with the most substantial reductions occurring in the 4.75–6.7 mm size class, suggesting breakdown of dense, composite particles into more separable size-density fractions.

Attrition also redistributed particle sizes, shifting mass from the coarser fraction (>4.75 mm, down from 41.7% to 26.5%) to the intermediate range (especially the 2–4.75 mm and 1–2 mm classes), which increased from 20.9% to 28.5% and 12.4% to 15.8%, respectively. This redistribution is favorable for downstream density-based separation. The <0.5 mm fraction rose only modestly, from 17.2% to 18.9%, indicating controlled generation of fines during attrition. Extending attrition from 2

 doi:10.20944/preprints202505.0954.v1



to 5 minutes resulted in diminishing returns. The RD ≤ 1.3 fraction increased only slightly to 14.8%, while the ≥ 1.8 RD fraction decreased marginally to 20.5%. Redistribution was more apparent within intermediate-density classes (1.3–1.5 RD), suggesting further disintegration of partially liberated particles, but with limited new liberation of clean coal. The <0.5 mm fraction increased to 20.7%, reflecting ongoing surface abrasion that could lead to handling challenges and lower recovery in fine circuits. When comparing across top sizes, it is evident that initial breakage to 6.7 mm followed by 2 minutes of attrition is the most effective strategy for maximizing liberation. At this condition, the RD < 1.4 fraction reached 39.3%, versus 25.1% at 13.2 mm with the same attrition time. Likewise, the <0.5 mm fraction increased from 11.1% (13.2 mm) to 18.9% (6.7 mm) after attrition, confirming that finer particles promote greater surface exposure and attrition response.

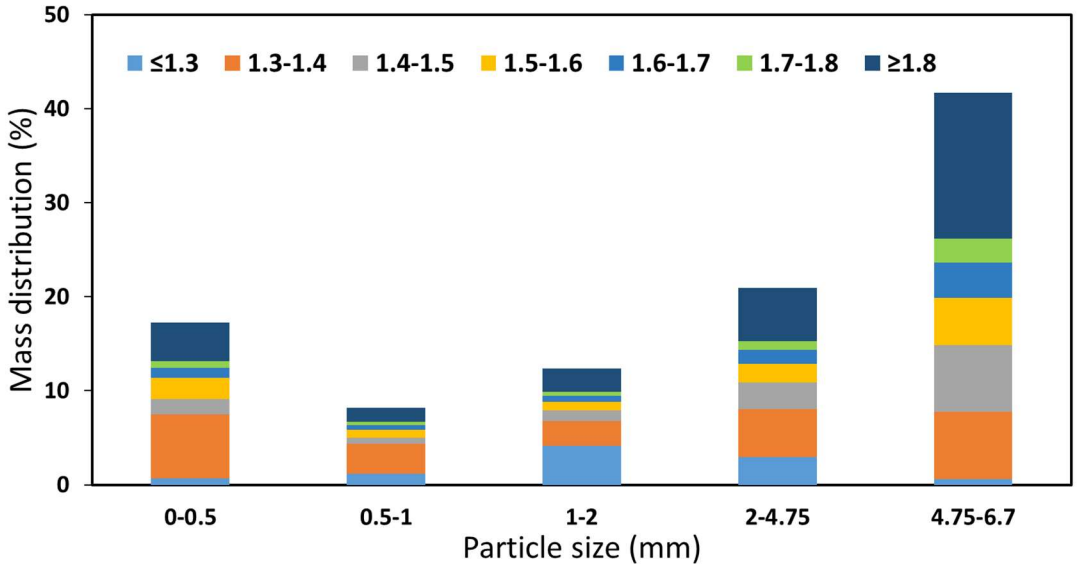


**Figure 8.** Size-by-washability distribution of coal subjected to impact breakage to a top particle size of 6.7 mm, without any additional attrition treatment.

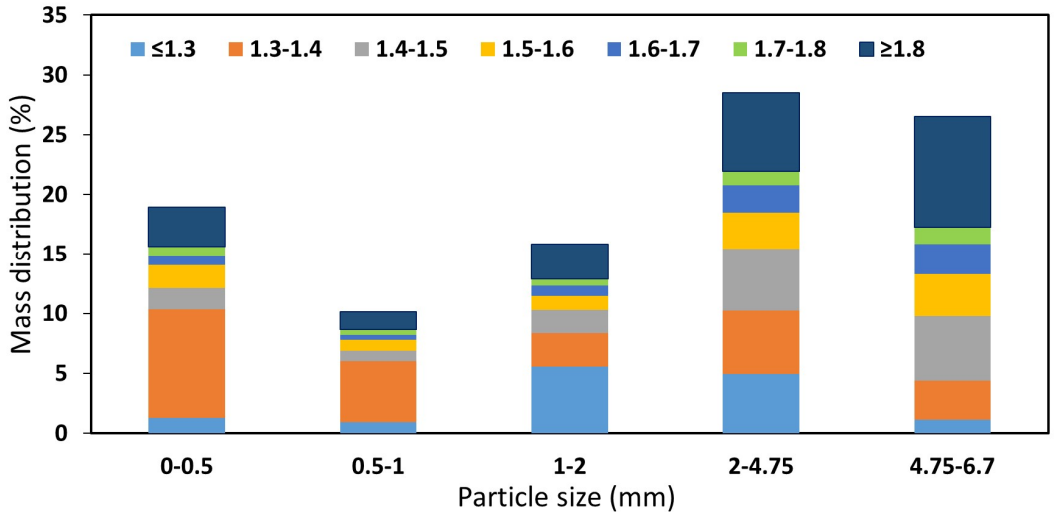


**Figure 9.** Size-by-washability distribution of coal subjected to impact breakage to a top particle size of 6.7 mm, followed by 2 minutes of attrition breakage.

 doi:10.20944/preprints202505.0954.v1



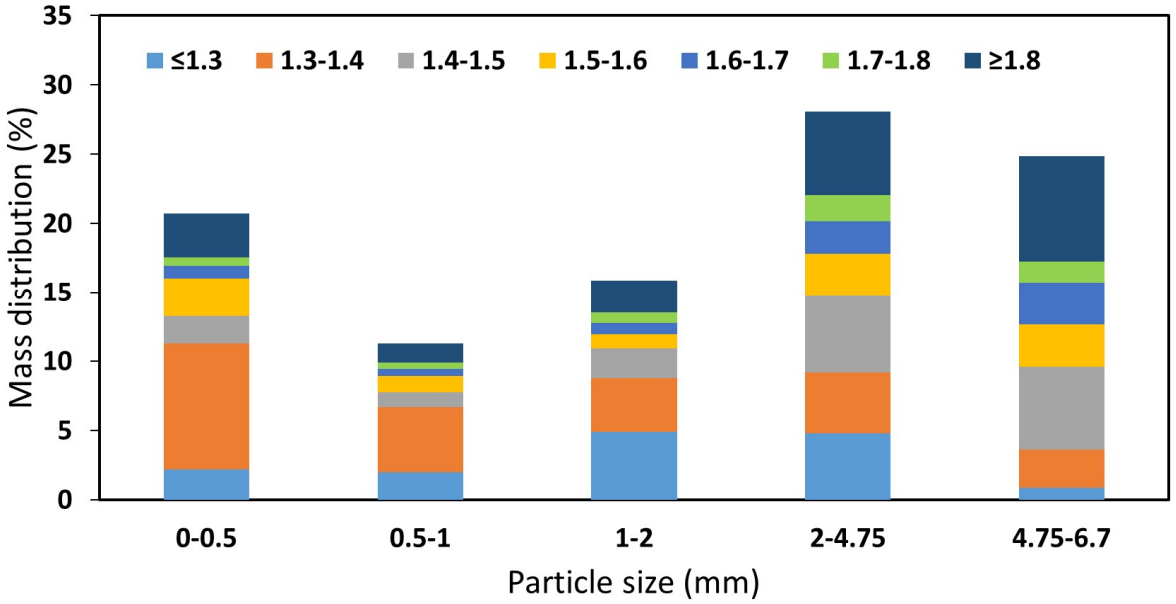


**Figure 10.** Size-by-washability distribution of coal subjected to impact breakage to a top particle size of 6.7 mm, followed by 5 minutes of attrition breakage.

### *3.2. Effect of Compressive and Attrition Breakage on Size-by-Washability Distribution*

#### 3.2.1. Top Particle Size of 13.2 mm

Figures 11–13 summarize the washability response of coal subjected to compressive breakage down to a top particle size of 13.2 mm, followed by 0, 2, and 5 minutes of attrition.

Initial compressive breakage without attrition achieved moderate liberation, with 6.92% of the sample reporting to the RD ≤ 1.3 category. As with impact breakage, these low-density particles were primarily concentrated in the 1–4.75 mm range, indicating that compressive forces favor the production of intermediate-size liberated coal rather than excessive fines.

The high-density fraction (RD ≥ 1.8) constituted 27.93% of the total mass and was concentrated predominantly in the 6.7–13.2 mm size range, highlighting the structural robustness of mineral aggregates under compressive stress. Notably, the portion of high-density material in the coarsest fraction (9.5–13.2 mm) was only 9.80%, substantially lower than the 17.85% observed under impact breakage. This suggests that compressive breakage is more effective at fracturing mineral-rich particles, potentially due to the generation of internal stress fields at contact points that promote fragmentation.

Fines (<0.5 mm) accounted for 14.19% of the total mass—higher than the 10.7% observed after the impact breakage. This increase may be attributed to localized abrasion and micro-cracking during compression. Nevertheless, fines generation remained within acceptable operational limits.

The total liberated fraction (RD ≤ 1.4) was 29.20%, higher than the 25.2% achieved by impact breakage, primarily due to an elevated 1.3–1.4 RD component (22.33%). In contrast, the RD ≤ 1.3 fraction remained comparable between breakage modes. This suggests compressive stress facilitates broader exposure of maceral-mineral boundaries but does not necessarily release the most floatable coal without additional treatment.

Following 2 minutes of attrition, the RD ≤ 1.3 fraction increased to 8.20%, while the total RD ≤ 1.4 content rose to 31.47%. This confirms that attrition efficiently promotes maceral liberation by exploiting micro-fractures introduced during compressive breakage. Most of the improvement occurred within the intermediate size fractions, where pre-existing cleavage planes allowed for disaggregation. Compared to the impact breakage case at the same attrition time (32.8% RD ≤ 1.4), compressive breakage yielded slightly lower liberation, possibly due to reduced exposure of fresh surfaces for attrition to act upon. This underscores the complementary role of breakage mechanism and attrition efficiency. The RD ≥ 1.8 fraction decreased only marginally from 27.93% to 27.25%,

 doi:10.20944/preprints202505.0954.v1



indicating attrition had limited effect on mineral-rich particles. Fines increased to 16.81%, reflecting enhanced surface wear. However, the increase remained controlled, suggesting that short-duration attrition can enhance separation potential without severe overgrinding.

Extending attrition to 5 minutes yielded diminishing returns. The RD ≤ 1.3 fraction increased slightly to 8.60%, while the total RD ≤ 1.4 content reached 32.20%—a marginal gain of just 0.73 percentage points over the 2-minute treatment. Likewise, the high-density material (RD ≥ 1.8) declined slightly further to 26.40%.

Fine generation continued to rise, reaching 17.19%, underscoring the potential risk of excessive fines accumulation with prolonged attrition. This may negatively impact flotation recovery and increase moisture retention, thus complicating downstream handling.

Redistribution within the 1.4–1.5 and 1.5–1.6 RD classes was modest, suggesting that most partially liberated middlings had already transitioned during the 2-minute attrition stage. Further breakage mainly affected resistant composites, which tend to produce fines rather than floatable coal.

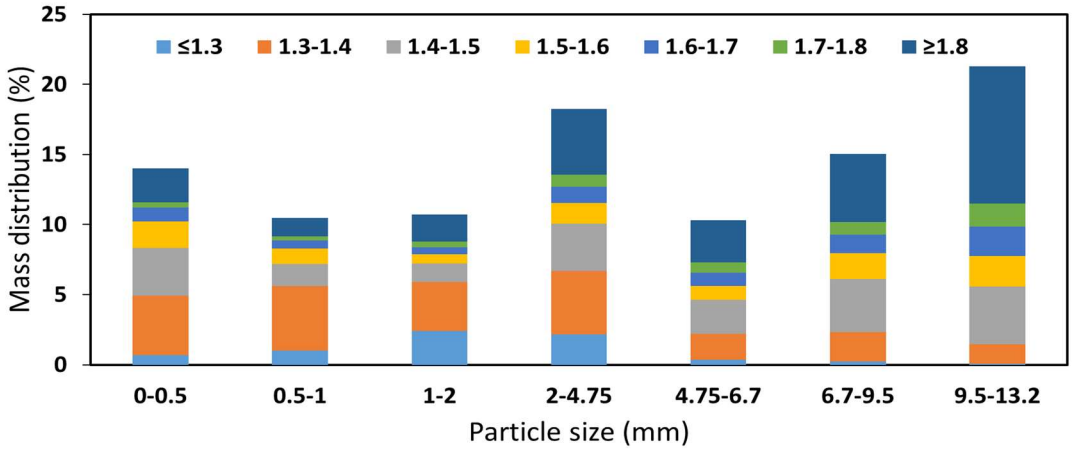


**Figure 11.** Size-by-washability distribution of coal subjected to compressive breakage to a top particle size of 13.2 mm, without any additional attrition breakage.

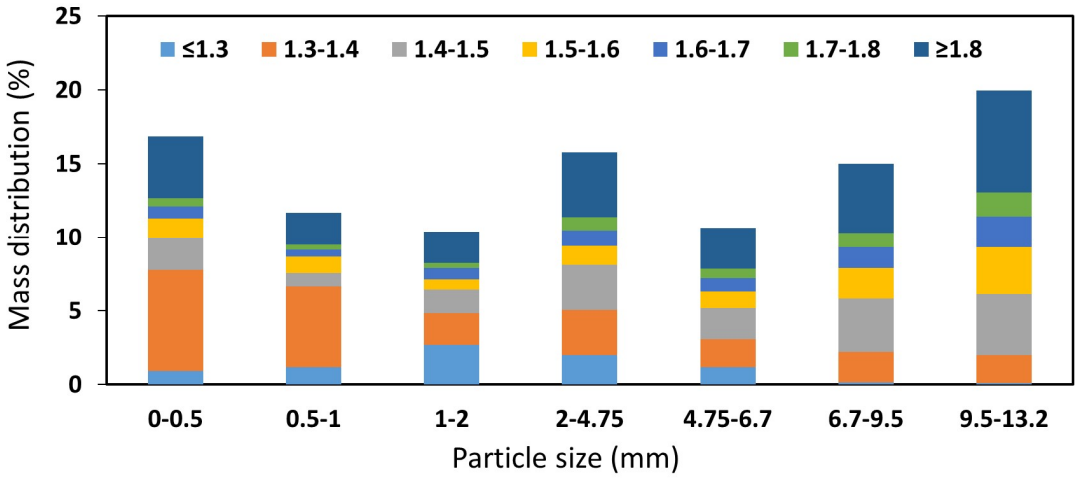


**Figure 12.** Size-by-washability distribution of coal subjected to compressive breakage to a top particle size of 13.2 mm, followed by 2 minutes of attrition breakage.

 doi:10.20944/preprints202505.0954.v1



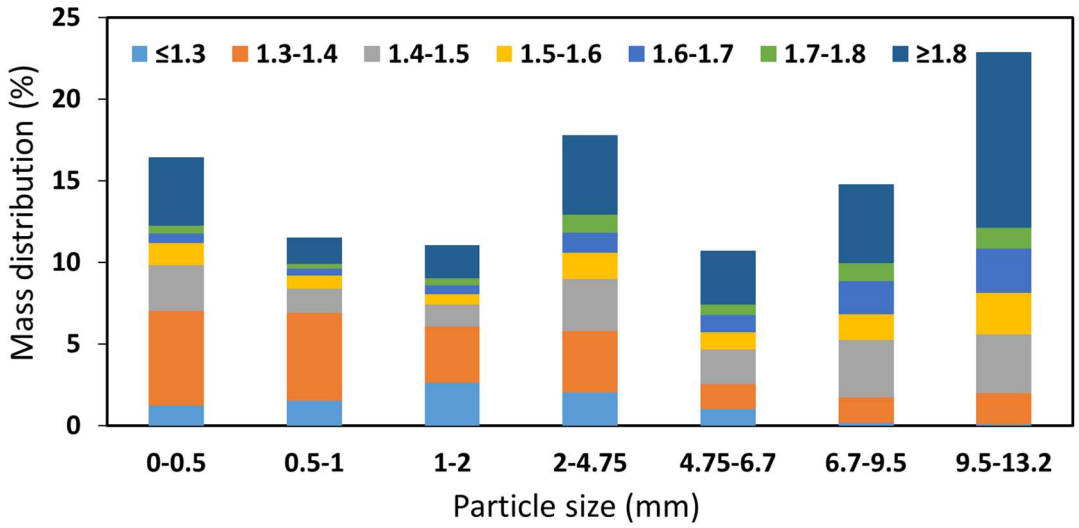


**Figure 13.** Size-by-washability distribution of coal subjected to compressive breakage to a top particle size of 13.2 mm, followed by 5 minutes of attrition breakage.

3.2.2. Top Particle Size of 6.7

Figures 14–16 present the size-by-washability data for coal subjected to compressive breakage to a top particle size of 6.7 mm, followed by 0, 2, and 5 minutes of attrition.

Compressive breakage without attrition produced 11.0% of coal in the RD ≤ 1.3 category—higher than the 9.6% observed after impact breakage at the same top size—suggesting that compressive stress more effectively promotes initial liberation of clean coal macerals. Most low-density particles were concentrated in the 0.5–4.75 mm size range, reflecting effective disaggregation into manageable sizes without excessive overgrinding.

The RD ≥ 1.8 fraction, indicative of mineral-rich material, accounted for 30.3% of the total mass. The 4.75–6.7 mm size fraction alone accounted for 32.6% of the total sample mass, within which 15.05% was composed of high-density material (RD ≥ 1.8). This supports the need for post-breakage treatment, such as attrition, to enhance liberation by detaching coal macerals from mineral matter within this size class. Fine generation (<0.5 mm) was also considerable, comprising 16.8% of the total, likely due to intergranular cracking and particle abrasion at contact points. Intermediate-density material (RD 1.4–1.8) made up approximately 38.6% of the mass, with the 1.4–1.5 RD class contributing the largest portion (15.9%).

Applying 2 minutes of attrition resulted in marked improvement in liberation. The RD ≤ 1.3 fraction increased to 15.4%, and the RD ≤ 1.4 total reached 34.4%, reflecting dislodgement of coal macerals via surface abrasion and the weakening of mineral-coal interfaces previously exposed during compressive breakage. This liberation was accompanied by a decline in the RD ≥ 1.8 fraction to 22.8%, suggesting fragmentation and size reduction of previously resistant mineral-rich particles.

Fine production rose slightly to 17.4%, and the coarse fraction (4.75–6.7 mm) decreased from 32.6% to 22.9%, confirming attrition's role in transitioning coarse middlings into finer, more separable fractions. These results affirm that short-duration attrition improves separation potential without excessively increasing the fine burden.

Extending attrition to 5 minutes provided diminishing returns. The RD ≤ 1.3 category increased only marginally to 16.3%, while the RD ≤ 1.4 total slightly declined to 32.7%, indicating a degree of redistribution into other density classes or minor mass loss due to fines formation. The RD ≥ 1.8 fraction remained nearly unchanged at 23.1%, suggesting minimal further benefit in terms of mineral liberation. Fines generation continued to increase, reaching 19.0%, and the coarse fraction further declined to 20.8%. This shift implies that prolonged attrition promoted continued particle surface degradation, potentially leading to the generation of mineral-rich fines that are difficult to dewater or recover.

 doi:10.20944/preprints202505.0954.v1



Interestingly, the 1.3–1.4 RD category declined from 18.9% (2 min attrition) to 16.6%, suggesting further separation of borderline middlings into either clean coal (≤ 1.3 RD) or denser fractions (≥ 1.4 RD). While this indicates continued liberation, it also reflects attrition's tendency to grind middlings into fine form when overapplied.

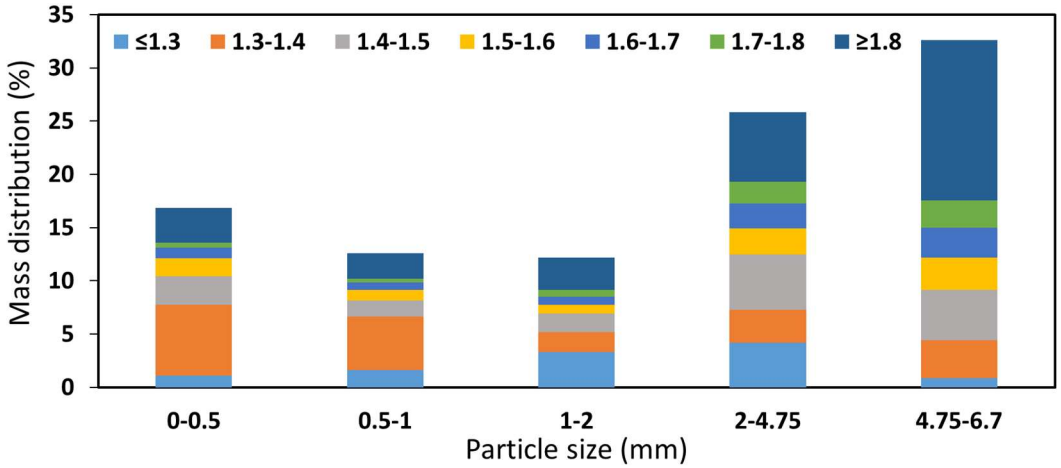


**Figure 14.** Size-by-washability distribution of coal subjected to compressive breakage to a top particle size of 6.7 mm, without any additional attrition breakage.

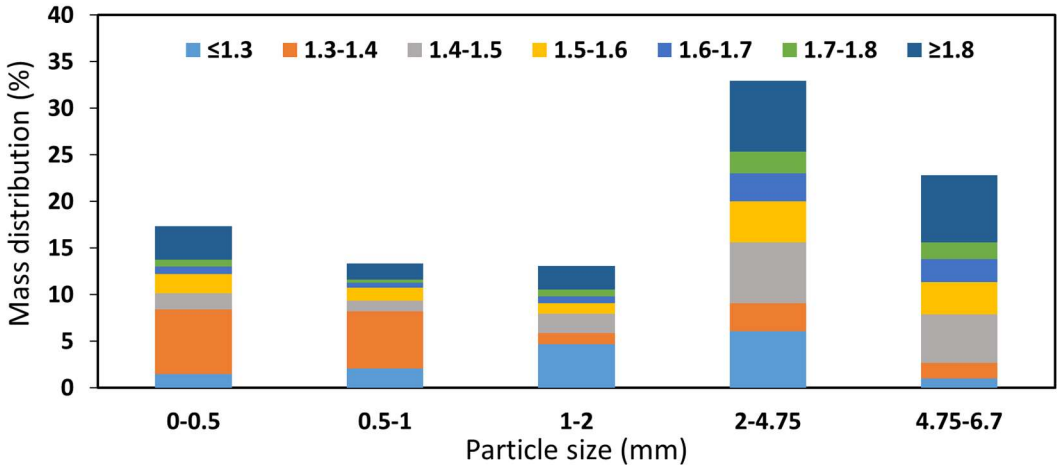


**Figure 15.** Size-by-washability distribution of coal subjected to compressive breakage to a top particle size of 6.7 mm, followed by 2 minutes of attrition breakage.

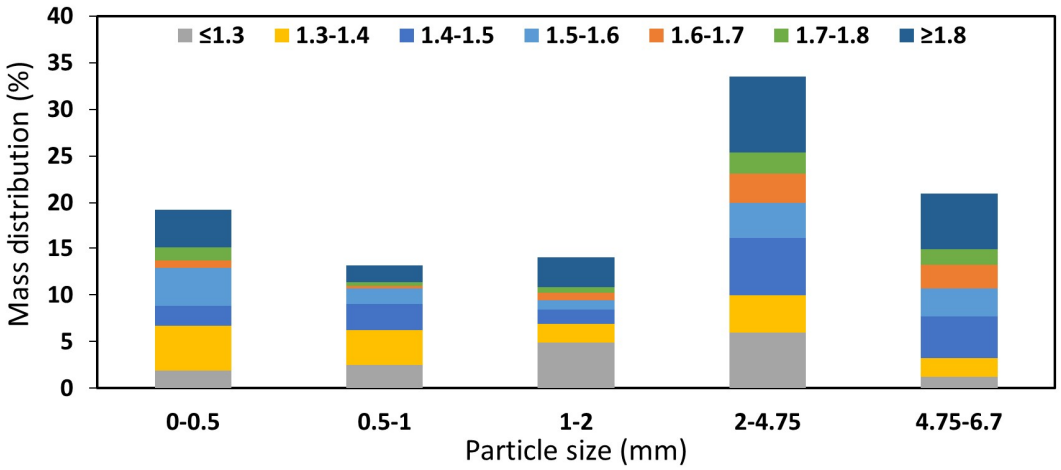

 doi:10.20944/preprints202505.0954.v1



**Figure 16.** Size-by-washability distribution of coal subjected to compressive breakage to a top particle size of 6.7 mm, followed by 5 minutes of attrition breakage.

A comparison of impact and compressive breakage at top sizes of 13.2 mm and 6.7 mm (each followed by 2 minutes of attrition) reveals distinct liberation patterns and fragmentation behavior. At 13.2 mm, impact breakage followed by attrition produced 32.8% low-density coal (RD ≤ 1.4), while compressive breakage yielded slightly less at 31.6%. However, impact breakage retained a higher proportion of dense, mineral-rich particles (RD ≥ 1.8 = 30.6%) compared to 27.3% under compressive stress, indicating that impact forces were less effective in fragmenting dense composites. On the other hand, compressive breakage generated more fines (16.8%) than impact breakage (11.1%), reflecting a higher tendency toward surface abrasion and intergranular cracking.

At the finer top size of 6.7 mm, both methods showed improved liberation. Impact breakage with attrition produced the highest yield of low-density material (RD ≤ 1.4 = 39.3%), outperforming compressive breakage at the same size (34.4%). However, this improved liberation under impact was accompanied by the highest fine generation (18.9%), compared to 17.5% for compressive breakage. Meanwhile, the high-density fraction decreased more significantly under compressive conditions (RD ≥ 1.8 = 22.8%) than under impact (23.6%), suggesting better disintegration of mineral aggregates. These findings indicate that for maximizing clean coal recovery, impact breakage to a top size of 6.7 mm followed by 2 minutes of attrition is the most effective strategy, offering the highest liberation despite a tradeoff in fine generation

Figure 17 presents the overall washability distribution of coal subjected to different breakage mechanisms—impact and compressive—at top particle sizes of 13.2 mm and 6.7 mm. The results clearly demonstrate that both the breakage method and target top particle size play a pivotal role in coal liberation and clean coal yield. Reducing the top particle size from 13.2 mm to 6.7 mm consistently enhanced liberation, regardless of whether impact or compressive breakage was used. For instance, clean coal yield at approximately 10% ash increased from 25.2% (impact at 13.2 mm without attrition) to 34.5% (impact at 6.7 mm without attrition), and further improved to 39.3% when attrition was added. Compressive breakage exhibited a similar trend: clean coal yield improved from only 6.9% at 13.2 mm (no attrition) to 31.2% at 6.7 mm (no attrition), and to 34.2% with 2 minutes of attrition. These results reflect the importance of size reduction for exposing maceral-mineral interfaces, particularly in coal samples characterized by complex intergrowths.

When comparing the two breakage modes, impact breakage demonstrated greater effectiveness in liberating floatable coal, particularly when combined with finer sizing and short-duration attrition. At a top size of 6.7 mm followed by 2 minutes of attrition, impact breakage achieved the highest cumulative float yield at ~10% ash (39.3%) and a relatively low final ash content of 27.4%. Compressive breakage under the same conditions achieved a slightly lower clean coal yield (34.2%) and higher final ash (28.3%). In contrast, compressive breakage was more effective in fragmenting high-density mineral-rich particles and reducing the proportion of coarse rejects, especially at coarser top sizes. However, it also produced more fines and delivered lower liberation at clean ash levels. Overall, the optimal strategy for maximizing clean coal yield while minimizing overgrinding and ash content is impact breakage to 6.7 mm followed by 2 minutes of attrition. This configuration offers the best balance of selective fragmentation, maceral liberation, and fines control, and is therefore recommended for high-efficiency coal beneficiation in plant-scale applications.

 doi:10.20944/preprints202505.0954.v1



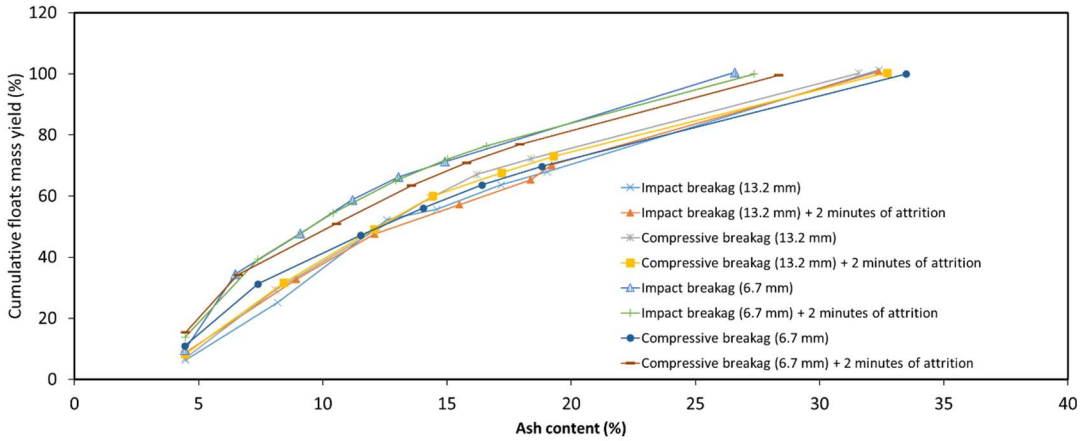


**Figure 17.** Overall washability distribution of coal subjected to different breakage mechanisms at top particle sizes of 13.2 mm and 6.7 mm.

## 4. Conclusions

This study systematically evaluated the influence of different breakage mechanisms—impact, compressive, and attrition—on the size-by-washability distribution and liberation behavior of coal samples sourced from the Moatize Coalfield in Mozambique. The findings clearly indicate that both the type of breakage mechanism and the target top particle size significantly affect the liberation of clean coal (RD ≤ 1.4) and the overall yield of low-ash material.

Reducing the top particle size from 13.2 mm to 6.7 mm consistently enhanced liberation across all breakage types. Impact breakage followed by 2 minutes of attrition yielded the highest proportion of low-density material (~39.5%), while maintaining moderate levels of ultrafine generation (<0.5 mm). Compressive breakage was found to be more effective in fragmenting mineral-rich, high-density particles and reducing coarse rejects, particularly at larger particle sizes. However, it also resulted in slightly higher ultrafine production and a lower proportion of highly liberated coal in the RD ≤ 1.3 range compared to impact breakage.

Attrition played a critical role in improving liberation, especially for intermediate-density fractions (RD 1.3–1.6), where maceral–mineral intergrowths were partially detached. A 2-minute attrition duration was generally optimal, enhancing liberation without excessive generation of ultrafines. Extending attrition time to 5 minutes offered diminishing returns and increased the risk of overgrinding and process inefficiencies. Future research should explore mineral liberation at the microstructural level using automated image analysis tools and investigate hybrid or staged breakage methods to further enhance efficiency while minimizing energy use and fine generation.

## References

1. Guldris Leon, L.; Bengtsson, M. Selective Comminution Applied to Mineral Processing of a Tantalum Ore: A Technical, Economic Analysis. Minerals 2022, 12, 1057.
2. Norgate, T.; Haque, N. Energy and Greenhouse Gas Impacts of Mining and Mineral Processing Operations. J. Clean. Prod. 2010, 18, 266–274.
3. Jeswiet, J.; Szekeres, A. Energy Consumption in Mining Comminution. Procedia CIRP 2016, 48, 140–145.
4. Shi, F.; Kojovic, T.; Larbi-Bram, S.; Manlapig, E. Development of a Rapid Particle Breakage Characterisation Device: The JKRBT. Miner. Eng. 2009, 22, 602–612.
5. Reedy, R.C.; Scanlon, B.R.; Bagdonas, D.A.; et al. Coal Ash Resources and Potential for Rare Earth Element Production in the United States. Int. J. Coal Sci. Technol. 2024, 11, 74.
6. Nakhaei, F.; Corchado-Albelo, J.; Alagha, L.; Moats, M.; Munoz-Garcia, N. Progress, Challenges, and Perspectives of Critical Elements Recovery from Sulfide Tailings. Sep. Purif. Technol. 2025, 354.
7. Bankefa, T.; Nasah, J.; Laudal, D.; Andraju, N. Advances in Efficient Utilization of Low-Rank Fuels in Coal and Biomass-Fired Systems: A Comprehensive Review. Energy Fuels 2024, 38, 10.

 doi:10.20944/preprints202505.0954.v1




8. Akinbami, O.M.; Oke, S.R.; Bodunrin, M.O. The State of Renewable Energy Development in South Africa: An Overview. Alex. Eng. J. 2021, 60, 5077–5093.
9. Botlhoko, S.; Campbell, Q.P.; Le Roux, M.; Nakhaei, F. Application of Rhovol Information for Coal Washability Analysis. In Proceedings of the Coal Processing Conference, Secunda, South Africa, 2021.
10. Botlhoko, S.; Campbell, Q.P.; Le Roux, M.; Nakhaei, F. Washability Analysis of Coal Using RhoVol: A Novel 3D Image-Based Method. Miner. Process. Extr. Metall. Rev. 2023, 44, 125–137.
11. Campbell, Q.P.; Le Roux, M.; Nakhaei, F. Coal Moisture Variations in Response to Rainfall Events in Mine and Coal-Fired Power Plant Stockpiles—Part 2: Evaporation. Minerals 2021, 11, 1366.
12. Fan, J.; Du, M.; Liu, L. Study on the Liberation of Organic Macerals in Coal by Liquid Nitrogen Quenching Pretreatment. Minerals 2020, 10, 911.
13. Hughes, N.; Le Roux, M.; Campbell, Q.P.; Nakhaei, F. A Review of the Dry Methods Available for Coal Beneficiation. Miner. Eng. 2024, 216, 108847.
14. Hornn, V.; Ito, M.; Yamazawa, R.; Shimada, H.; Tabelin, C.B.; Jeon, S.; Park, I.; Hiroyoshi, N. Kinetic Analysis for Agglomeration-Flotation of Finely Ground Chalcopyrite: Comparison of First-Order Kinetic Model and Experimental Results. Mater. Trans. 2020, 61, 1940–1948.
15. Zancan, P.M.; De Brum, I.A.S.; Ambrós, W.M.; Sampaio, C.H.; Moncunill, J.O. Influence of Igneous Intrusions on Coal Flotation Feasibility: The Case of Moatize Mine, Mozambique. Minerals 2023, 13, 161.
16. Hornn, V., Ito, M., Shimada, H., Tabelin, C. B., Jeon, S., Park, I., & Hiroyoshi, N. (2020). Agglomeration–flotation of finely ground chalcopyrite using emulsified oil stabilized by emulsifiers: Implications for porphyry copper ore flotation. Metals, 10(7), 912.
17. Seetharaman, S. (Ed.). (2014). Treatise on Process Metallurgy: Volume 3 – Industrial Processes. Elsevier.
18. Viljoen, J., Campbell, Q. P., Le Roux, M., & De Beer, F. (2015). An analysis of the slow compression breakage of coal using microfocus X-ray computed tomography. International Journal of Coal Preparation and Utilization, 35, 1–13.
19. Phengsaart, T., Srichonphaisan, P., Kertbundit, C., Soonthornwiphat, N., Sinthugoot, S., Phumkokrux, N., Juntarasakul, O., Maneeintr, K., Numprasanthai, A., Park, I., Tabelin, C. B., Hiroyoshi, N., & Ito, M. (2023). Conventional and recent advances in gravity separation technologies for coal cleaning: A systematic and critical review. Heliyon, 9(2), e13083.
20. O'Brien, G., Firth, B., & Adair, B. (2011). The application of the coal grain analysis method to coal liberation studies. International Journal of Coal Preparation and Utilization, 31(2), 96–111.
21. Falcon, L. M., & Falcon, R. M. S. (1987). The petrographic composition of Southern African coals in relation to friability, hardness, and abrasive indices. Journal of the South African Institute of Mining and Metallurgy, 87(10), 323–336.
22. Shi, F. (2014). Coal breakage characterization – Part 2: Multi-component breakage modelling. Fuel, 117, 1156–1162.
23. Kuwik, B. S., Garcia, M., & Hurley, R. C. (2022). Experimental breakage mechanics of confined granular media across strain rates and at high pressures. International Journal of Solids and Structures, 259, 112024.
24. Oberholzer, V., & Van der Walt, J. (2009). Investigation of factors influencing the attrition breakage of coal. Journal of the Southern African Institute of Mining and Metallurgy, 109(4), 211–216.
25. Wills, B. A., & Finch, J. A. (2016). Wills' Mineral Processing Technology: An Introduction to the Practical Aspects of Ore Treatment and Mineral Recovery (8th ed.). Butterworth-Heinemann.
26. Martinelli, G., Plescia, P., Tempesta, E., Paris, E., & Gallucci, F. (2020). Fracture analysis of $\alpha$-quartz crystals subjected to shear stress. Minerals, 10(10), 870.
27. Cleary, P. W., Delaney, G. W., Sinnott, M. D., Cummins, S. J., & Morrison, R. D. (2020). Advanced comminution modelling: Part 1 – Crushers. Applied Mathematical Modelling, 88, 238–265.
28. Moraga, C.; Astudillo, C.A.; Estay, R.; Maranek, A. Enhancing Comminution Process Modeling in Mineral Processing: A Conjoint Analysis Approach for Implementing Neural Networks with Limited Data. Mining 2024, 4, 966–982.
29. Parapari, P.S.; Parian, M.; Rosenkranz, J. Breakage process of mineral processing comminution machines – An approach to liberation. Adv. Powder Technol. 2020, 31, 3669–3685.

 doi:10.20944/preprints202505.0954.v1



30. Adewuyi, S.O.; Ahmed, H.A.M.; Ahmed, H.M.A. Methods of Ore Pretreatment for Comminution Energy Reduction. Minerals 2020, 10, 423.
31. Adewuyi, S.O.; Ahmed, H.A.M.; Anani, A.; Saeed, A.; Ahmed, H.M.; Alwafi, R.; Luxbacher, K. Enhancing Iron Ore Grindability through Hybrid Thermal-Mechanical Pretreatment. Minerals 2024, 14, 1027.
32. Kingman, S.W. Recent developments in microwave processing of minerals. Int. Mater. Rev. 2006, 51, 1–12.
33. Heshami, M.; Ahmadi, R. Effect of thermal treatment on specific rate of breakage of manganese ore. J. Min. Environ. 2018, 9, 339–348.
34. Wonnacott, G.; Wills, B.A. Optimisation of Thermally Assisted Liberation of a Tin Ore with the Aid of Computer Simulation. Miner. Eng. 1990, 3, 187–198.
35. Toprak, N.A.; Altun, O.; Aydogan, N.; Benzer, H. The influences and selection of grinding chemicals in cement grinding circuits. Constr. Build. Mater. 2014, 68, 199–205.